Magnetic properties of ultrathin discontinuous Co/Pt multilayers: Comparison with short-range ordered and isotropic CoPt_{3} films

M. Charilaou, C. Bordel, P.-E. Berche, B. B. Maranville, P. Fischer, and F. Hellman

Phys. Rev. B **93**, 224408 — Published 7 June 2016

DOI: 10.1103/PhysRevB.93.224408

Magnetic properties of ultrathin discontinuous Co/Pt multilayers: comparison with short-range ordered and isotropic $CoPt_3$ films

M. Charilaou,[1,2,3] C. Bordel,[1,2,4] P.-E. Berche,[4] B. B. Maranville,[5,*] P. Fischer,[1,6] and F. Hellman[1,2,5,†]

[1] *Materials Sciences Division, Lawrence Berkeley National Laboratory, Berkeley, CA 94720, USA*
[2] *Department of Physics, University of California Berkeley, Berkeley, CA 94720, USA*
[3] *Department of Materials, ETH Zurich, 8093 Zurich, Switzerland*
[4] *GPM, UMR 6634 CNRS-Université de Rouen, 76801 St. Etienne du Rouvray, France*
[5] *Department of Physics, University of California San Diego, San Diego, CA 92093, USA*
[6] *Department of Physics, University of California Santa Cruz, Santa Cruz, CA 94056, USA*

Magnetic properties of thin (Co/Pt) multilayers have been investigated in order to study the dependence of magnetization M, uniaxial anisotropy K_u, and Curie temperature T_C on the multilayer thickness, composition and structure. A comparison between epitaxial sub-monolayer multilayers and epitaxial fcc $CoPt_3$ alloy films with large perpendicular magnetic anisotropy (PMA) attributed to growth-induced Co clustering reveals significant differences in the temperature dependence of magnetization $M(T)$, despite the presence of thin planar Co platelets in both cases. Even the thinnest discontinuous multilayered structure shows a Langevin-like $M(T)$, while the alloy films with PMA show a broadened and enhanced $M(T)$ indicating a distribution of environments, including monolayer Co platelets separated by only 1–2 layers of Pt. These differences have been reproduced in Monte Carlo simulations, and are shown to be due to different distributions of Co-Co and Co-Pt nearest neighbors. The relatively uniform Co-Co coordination of even a discontinuous rough multilayer produces a Langevin-like $M(T)$, whereas the broader distribution associated with platelets in the PMA films results in a nearly linear T-dependence of M.

PACS numbers: 75.10.Hk, 75.30.Gw, 75.40.Mg, 75.70.Cn
Keywords: Co/Pt multilayers, perpendicular anisotropy, magnetometry, Monte Carlo

I. INTRODUCTION

Since the first reports on perpendicular magnetic anisotropy in (Co/Pt) multilayers[1,2], this system has attracted an uninterrupted interest. The literature spans an extremely broad range of topics including interface effects[3,4], perpendicular magnetic anisotropy[5–9], domain pattern and magnetization reversal[10–16], magneto-optical properties[17–20], interlayer coupling[21,22], magnetotransport properties[23–25], exchange biasing[26,27], spin injection[28], spin-polarization[29,30], spin-torque[31,32], magnetic recording[33–35], current-driven domain walls[36,37], and skyrmions[38–42].

Thin (Co/Pt) multilayers exhibit significant PMA[43,44] due to asymmetries in the interfacial bonding, crystallographic orientation or magnetoelastic strain. It has also been shown, however, that under certain growth conditions (substrate temperature of 450–725 K), Co-Pt alloy films with a range of compositions, both epitaxial with various orientations *and* polycrystalline, *also* possess PMA[45–48], despite an apparently cubic (fcc) structure evidenced by both X-ray and electron diffraction. In addition to PMA, these alloy films exhibit a large increase in the Curie temperature and saturation magnetization M_s, along with a very stretched, non-Langevin like $M(T)$. All of these effects in the PMA alloy films have been ascribed to growth-induced Co clustering, which causes an increase in Co-Pt out-of-plane coordination and Co-Co in-plane coordination, *i.e.* an oriented short-range order (o-SRO) of Co platelets that *locally* resembles a multilayer[49,50]. These o-SRO films have uniaxial anisotropy that approaches that of the best multilayers, and an enhanced magnetization and Curie temperature; these properties result from the clustering and oriented chemical order, and go away on annealing.

Direct observation of the o-SRO Co platelets (embedded in a coherent epitaxial fcc Pt-rich alloy) has proven challenging but EXAFS experiments support the model of thin small Co platelets, and suggest a size of order of 1 monolayer (ML) thick and 10 Å wide[49,50]. Growth simulations have suggested that this locally multilayer-like environment results from Co segregation to step edges during growth[51]. This metastable o-SRO structure does not conform to any phase of the equilibrium phase diagram and is a direct consequence of the growth process[51]. When the o-SRO alloy films are annealed at high temperature and then quenched, the PMA and enhanced M and T_C disappear and the films convert to one of the equilibrium bulk phases[46], *i.e.* the long-range-ordered (LRO) phase $L1_2$ (Cu_3Au) structure if annealed below 960 K or the chemically disordered face-centered cubic (fcc) structure if annealed above the order-disorder temperature of 960 K[52].

(Co/Pt) multilayers with Co layers in the sub-ML limit may be expected to have a structure similar to that of the small thin platelets of the o-SRO alloy films. The comparison between the two can therefore shed light both on the still incompletely-understood magnetization of the o-SRO films and their enhanced and broadened $M(T)$ and T_C, as well as on the physics of magnetic order and anisotropy in the ultrathin limit. Although surface analyses have been carried out on ultrathin Co overlayers de-

posited on a single-crystalline Pt layer[53–55], little attention has been dedicated to the temperature dependence of the magnetization in the ultrathin limit of (Co/Pt) multilayers, where coupling between Co layers and polarization of the thin Pt layer are expected to play a particularly significant role[43,44]. We here present the magnetic properties of (Co/Pt) multilayers with individual layer thicknesses ranging between 1.5 – 6 Å (0.75 – 3 ML) Co and between 3.1 – 49.6 Å Pt (1.5 – 22 ML).

The results obtained on the multilayer with the thinnest bilayer with a 1:3 Co:Pt composition are compared to the results for a $CoPt_3$ alloy film with PMA due to its oriented short-range order (o-SRO) and that of a random fcc $CoPt_3$ alloy. We also performed Monte Carlo simulations on these three systems to get $M(T)$ for Co-Pt systems (multilayers of varying roughness, alloys with various platelet-type structures embedded, and random alloys), focusing on an overall Co:Pt ratio of 1:3. By determining the relationship between the physical structure, the Curie temperature and the temperature dependent magnetization of the films, we gain insight into the local environment of Co and Pt atoms in the metastable o-SRO $CoPt_3$ alloy films with PMA.

II. SAMPLE PREPARATION

Epitaxial (111)-oriented multilayers were prepared by electron beam evaporation of Co and Pt under ultrahigh vacuum conditions, at a deposition rate of approximately 0.1 Å/s and a base pressure of $< 1 \times 10^{-9}$ Torr. In order to achieve good epitaxy, a 100 Å Pt seed layer was grown on (0001) sapphire substrates prior to sample deposition. Films were grown at 420 K in order to minimize intermixing of Co and Pt, while still giving good epitaxy of fcc Co and Pt. Computer-controlled shutters were used with feedback from crystal rate monitors to give precise layer thickness control. Reflection high-energy electron diffraction (RHEED) patterns obtained *in situ* confirmed the epitaxial growth.

Nine (Co/Pt) multilayers were grown, with layer thicknesses and overall compositions shown in table 1. For reference, one monolayer of (111)-oriented fcc Co is 2.06 Å thick, while a monolayer of (111)-oriented fcc Pt is 2.27 Å thick. Some films were annealed after growth at 1073 K and then quenched to 300 K to give chemically disordered fcc Co-Pt alloy films, where their T_C and M_s at low T confirmed their composition. The total thickness of each film is 650 Å.

Co:Pt	Co (Å)	Pt (Å)	Nr. of bilayers
1:1.5	1.5	3.1	141
	3	6.2	71
	6	12.4	35
1:3	1.5	6.2	84
	3	12.4	42
	6	24.8	21
1:6	1.5	12.4	47
	3	24.8	23
	6	49.6	12

TABLE I. Overall composition, individual layer thickness and number of bilayers of the nine Co/Pt multilayers fabricated and studied.

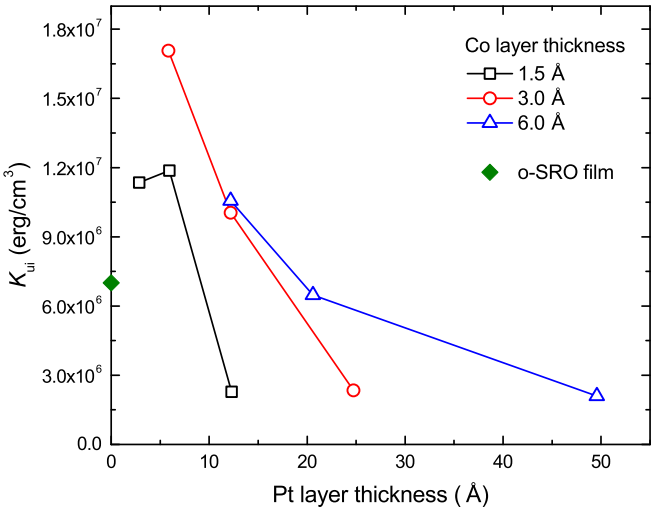

FIG. 1. Intrinsic uniaxial magnetic anisotropy at 300 K vs. Pt layer thickness for Co/Pt multilayers with various Co layer thicknesses.

III. EXPERIMENTAL RESULTS

Torque magnetometry was used to determine the magnitude of PMA at 300 K, using a field of 21 kOe and varying the angle of the field relative to sample normal to determine the uniaxial anisotropy energy, K_u. The shape anisotropy contribution of $2\pi M_s^2$ was corrected, to give the intrinsic uniaxial magnetic anisotropy K_{ui}, plotted vs. Pt interlayer thickness in Figure 1 for different Co layer thicknesses. Data is here shown in energy density rather than normalized to the interfacial area to enable comparison to the alloy films. All multilayers exhibit perpendicular magnetic anisotropy, which is found to strongly decrease as a function of the thickness of the Pt layers; PMA is an interfacial effect so this result is expected. PMA depends also on Co layer thickness, but this effect is convolved with a reduced T_C (to be discussed below) for thinner Co.

For comparison, o-SRO films at 1:3 ratio have magnetic anisotropy of 7×10^6 erg/cm^3 at room temperature[46]. This value is striking, considering that it is comparable to that of the three multilayers with similar overall 1:3 composition (ranging from 1.2×10^7 to 6×10^6 erg/cm^3). The strong PMA in the o-SRO film is most probably due to the increased overall Pt/Co interface area, which enhances the anisotropy[56], and it is comparable to that measured in textured multilayers[57].

The saturation magnetization M_s [from $M(H)$ extrap-

olated from high field to $H = 0$], measured by vibrating sample magnetometry (VSM) at 300 K, is shown in Fig. 2, plotted vs. the averaged Co concentration for the multilayers as well as the o-SRO and random fcc $CoPt_3$ films. M_s vs Co layer thickness of all samples with an average composition of 25 at.% Co are plotted as an inset of Fig. 2; the o-SRO and random fcc $CoPt_3$ alloy films are shown at zero Co layer thickness. The low M_s for the 14 at.% Co random fcc alloy at 300 K is due to its low T_C; for all other samples M_s at 300 K is within 10% of M_s at low T, due to their higher T_C. In Co-Pt materials, the moment contains contributions from Co spin and orbital contributions, as well as an induced Pt moment[58,59]. Co orbital contributions arise from incomplete quenching at interfaces, and has been previously linked to PMA[5]. Pt spin polarization is significant when Pt has Co neighbors, and leads even dilute Co-Pt alloys to be ferromagnetic with large moments per Co atom, with low T_C[60]. It has been previously noted[45] that M_s for the o-SRO film is significantly larger than that of a fully disordered $CoPt_3$ film (and even higher than that of an $L1_2$ phase $CoPt_3$ film); this effect can almost but not quite be explained by including all of the above contributions.

It is striking that no such enhancement is seen in any of the multilayered films. We observe a small increase in M_s as the bilayer thickness is reduced, but even for the thinnest bilayer (1.5 Å Co/3 Å Pt), which might be expected to have the greatest Co orbital moment and Pt polarization, M_s is not as high as for the o-SRO film and instead matches the value of a disordered fcc $CoPt_3$ film.

We here suggest that this increased M_s for the o-SRO alloy compared to the multilayers and to the random alloy is because the platelets in the o-SRO alloy have a greater number of edge Co atoms, which have a higher magnetic moment than even a surface Co atom[61], suggesting that the finite diameter of the platelets is an important factor to consider.

The T_C of the films, obtained by VSM measurement of the temperature dependence of remanent magnetization at $H = 0$, is plotted in Fig. 3 vs. Pt layer thickness for various Co layer thicknesses. Note that the upper temperature measured (700 K) is low enough that no significant change in M or K_u was found after the measurement, meaning that the structure was not altered by the measurement process. The corresponding values for a disordered sample of the same average composition are noted as purple stars on the left axis of the plot. Dotted lines join samples with the same Co:Pt ratio, while solid lines join samples with the same Co layer thickness. By following the data along the dashed lines of constant composition, we note first for the composition Co:Pt = 1:3, T_C of the multilayers is well above that of the random alloy (and far above that of the $L1_2$ phase), which is not surprising since the number of Co-Co nearest neighbors is higher, but well below that of the o-SRO alloy ($T_{onset} > 670$ K) for all except the thickest Co layer. By following the data along the solid lines of constant Co thickness, especially for the thinner Co thickness layers

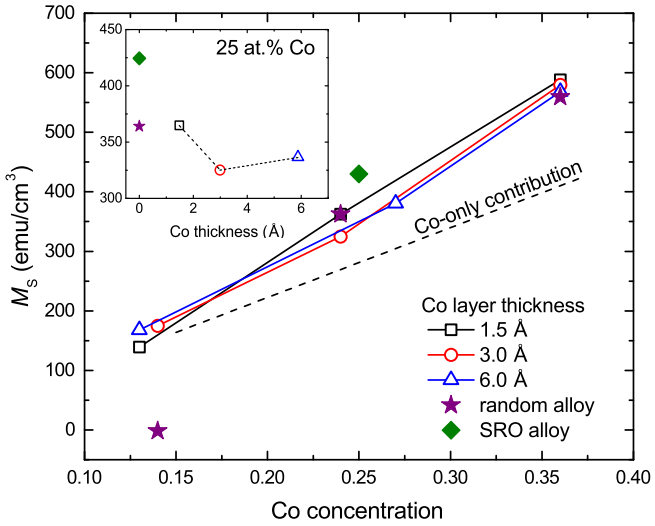

FIG. 2. Saturation magnetization M_s measured at 300 K vs. average Co concentration for the multilayers; data is also shown for the random fcc (purple stars) and o-SRO (green diamond) Co-Pt alloys (also at 300 K). The dotted line represents the contribution from the equivalent volume of pure Co. Inset shows M_s of films with 25 at.% Co vs. Co layer thickness; the random alloy and o-SRO film are shown on the zero Co thickness axis.

of 1.5 Å but also 3.0 Å, we see that the Pt layer thickness (hence the Co-Co interlayer spacing) strongly affects T_C (from 700 K down to 400 K with increasing Pt thickness). These thin (1.5 or even 3 Å) Co layers are not thick enough to support a high T_C in the absence of interlayer coupling, unlike the thicker (6 Å Co) films for which T_C remains fairly constant even for large Pt layer thickness (49.6 Å).

We here summarize the key experimental results. Comparing (Co/Pt) multilayers with o-SRO films, our experiments show that the PMA and T_C are comparable when the Co thickness is 1.5 to 6 Å and the Pt thickness is 15 Å or less. Specifically, to have comparable PMA and T_C, thin Co layers (1.5-3 Å) need to be separated by only 1-2 layers of Pt, while thicker layers (6 Å) have comparable T_C for all thicknesses of Pt, but their PMA is then lower. These results argue that many of the platelets in the o-SRO films are therefore 1-2 layers of Co, separated by 1-2 layers of Pt. We note that the overall composition of 1:3 means that there are other platelets separated by greater amounts of Pt, leading to the observed breadth of $M(T)$; only its onset is at 700 K. The enhanced M of the o-SRO, however, is not matched by any of the multilayers; this is suggested to be because the planar clusters of the o-SRO alloys have significantly more Co edge atoms with higher atomic magnetic moment than do the multilayers, despite the fact that they are sub-monolayer.

To gain insight into the origin of the differences between the o-SRO films and the ultrathin multilayers of the same composition, we focus on the Co:Pt 1:3 composition. Table 2 shows saturation magnetization M_s (re-

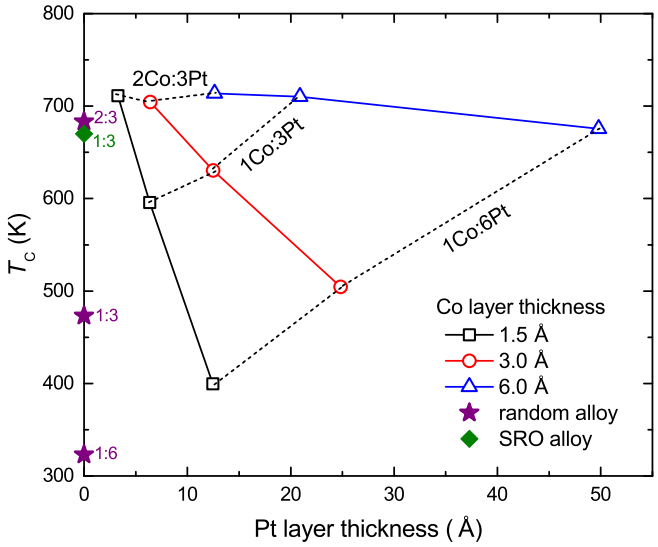

FIG. 3. T_C vs. Pt layer thickness for (Co/Pt) multilayers of various compositions (legend shows Co layer thickness, composition shown with dotted lines). The corresponding composition random fcc alloys are shown on the y-axis (purple stars), as is the o-SRO 1:3 PMA alloy (green diamond).

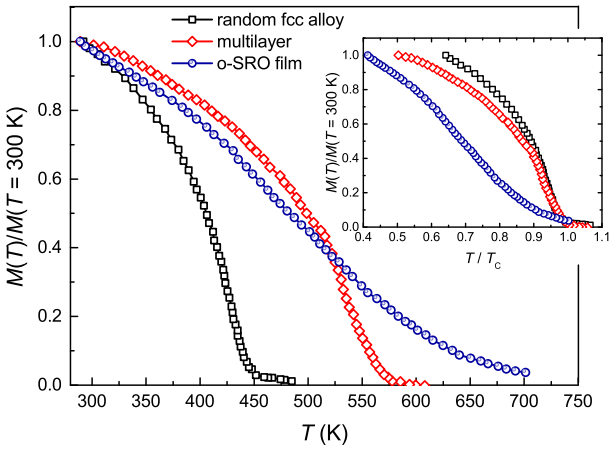

FIG. 4. Experimental remanent magnetization M (normalized to the room temperature value) vs T for the random fcc alloy (black squares), the (Co 1.5 Å/Pt 6.2 Å)$_{84}$ multilayer (red diamonds), and o-SRO $CoPt_3$ film (blue circles). The inset shows $M(T)$ for the three samples with T normalized to the T_C of each film.

ported at 5 K to avoid convolving effects of reduced T_C), Curie temperature T_C and intrinsic magnetic anisotropy K_{ui} of 4 films.

Even though PMA is a feature shared by thin (Co/Pt) multilayers and o-SRO $CoPt_3$ films, as previously discussed, their M_s, $M(T)$, and T_C are significantly different. The difference is most obvious in the M vs. T measurement, shown in Fig. 4. $M(T)$ is determined by VSM measurements of the magnetization along the easy axis of each film (out of plane for the multilayer and o-SRO film, and in plane for the random fcc alloy) after removing the applied field that was used to fully magnetize the samples at 300 K. The relatively large coercivity in these films makes remanent $M(T)$ be a meaningful measurement, until quite close to T_C. Figure 4 shows the normalized remanent magnetization $[M(T)/M(300\ \text{K})]$ vs. absolute temperature for the (Co 1.5 Å/Pt 6.2 Å)$_{84}$ multilayer, the o-SRO $CoPt_3$ film and the disordered fcc $CoPt_3$ film. The multilayer and disordered fcc sample show a Langevin-like behavior typical of a homogeneous ferromagnet (see inset to Fig. 4, where data is normalized to T_C of each film). In contrast, the data from the o-SRO film of $CoPt_3$ shows a very broad transition, indicating a distribution of T_C. Besides the significant difference in shape, we also note the persistence of remanent magnetization of the o-SRO sample to high temperature (nearly 700 K). This reflects a distribution of Co environments in the o-SRO sample, with small Co clusters leading to a high Curie temperature[50].

Sample	M_s (emu/cm^3)	T_C (K)	K_{ui} (erg/cm^3)	K_{eff} (erg/cm^3)
Co/Pt multilayer (1.5 Å/6.2 Å)	360	570	1.2×10^7	1.1×10^7
o-SRO $CoPt_3$	430	670	7×10^6	5.8×10^6
fcc $CoPt_3$	360	475	0	-8.1×10^5
L1$_2$ $CoPt_3$	300	290	0	-5.6×10^5

TABLE II. Experimental values of saturation magnetization (M_s) at 5 K, Curie temperature (T_C), intrinsic uniaxial anisotropy constant (K_{ui}), and effective anisotropy ($K_{\text{eff}} = K_{ui} - 2\pi M^2$) at 300 K for the (Co 1.5 Å /Pt 6.2 Å)$_{84}$ multilayer, o-SRO, random fcc, and L1$_2$ phase $CoPt_3$ alloys. T_C for the o-SRO alloy was taken as the temperature at which M exhibits an onset (more than 5% of the saturation M_s), with an uncertainty of ±10 K.

Thus, although these multilayers in the ultrathin limit seemingly should have been very similar to o-SRO $CoPt_3$ alloys, their experimental magnetization is quite different, indicating that the distribution of Co atomic environments is quite different.

Note that similar results have been found for a different composition alloy: $Co_{0.35}Pt_{0.65}$, which also shows PMA[46]. For that composition also, $M(T)$ is notably broad for films deposited near 670 K, while the films deposited at both higher and lower temperatures exhibit a sharp and nearly identical $M(T)$ dependence, with different T_C reflecting the different chemical ordering as for the $CoPt_3$ films.

To gain insight into the role played by the local magnetic environment of the Co atoms, we turned to numerical simulations. They have the advantage, over experiments performed on real samples, of allowing (i) a highly controlled variation of a physical parameter, like the lateral size and thickness of the Co platelets, and (ii) an easy access to local quantities like the coordination, its distribution, and the pair ordering. Additionally, the use of the Monte Carlo technique enables to simulate

the effect of temperature, which is key to understanding the difference in $M(T)$ behavior between the discontinuous multilayers and the short-range-ordered alloys of the same composition.

IV. MONTE CARLO SIMULATIONS: DETAILS

For the simulations, we focused on the 1:3 Co:Pt composition, specifically the sub-ML multilayer with varying degrees of roughness, the chemically-random fcc alloy, and an fcc structure with small flat Co platelets in a Pt-rich matrix to simulate the o-SRO films with PMA. All simulation samples consist of 25% Co atoms and 75% Pt atoms occupying the sites of an fcc lattice with (111) surfaces. For the multilayers, we included varying degrees of roughness, both because this is more realistic than perfect multilayers and because the experimentally-observed multilayers have a T_C well below that of pure Co, even for relatively thick Co layers, a result that can only be reproduced by including roughness. The thin multilayers were designed to be less than a full monolayer, matching experimental multilayers, which were intended to better simulate the platelets of the o-SRO films (the sub-ML structure with thickness 1.5 Å corresponds to 72% of the full thickness of a (111) ML).

Examples of these microstructures are shown in Fig. 5. The random alloy (Fig. 5a) has Co and Pt randomly occupying sites of the fcc lattice. To construct the sub-ML multilayer (Fig. 5b), we start with a perfect multilayer structure with Co/Pt/Pt/Pt repetition, and randomly swap 28% of the Co atoms with a Pt atom, maintaining the 1:3 overall composition. The roughness was implemented by substituting Co atoms in the Co-layer with Pt atoms, and relocating the substituted Co atoms randomly in the Pt layers. The generation of the microstructure of the o-SRO film (Fig. 5c) was done following the model suggested by the step-edge segregation model[51] and the findings of EXAFS experiments[50], *i.e.*, planar Co platelets ≈10 Å wide embedded in a Pt matrix. We simulated planar 2D Co platelets consisting of n atoms, with n ranging from 3 to 33, randomly distributed in the lattice. To create this, we begin with an fcc film with (111) orientation fully occupied with Pt. Based on the size of the platelets, *i.e.* the number n, we calculate the number of platelets N in the simulation structure, to yield an overall composition of 25 at.% Co. Next, we randomly select N sites that will be the centers of the platelets, and at these selected sites we substitute Pt with Co. Finally, we substitute Pt with Co on the requisite number of sites around the N seeds to yield n-atom clusters. Figure 5c shows $n = 15$, which has 1-2 Co on lattice sites in each lateral dimension surrounding the selection site, resulting in the formation of roughly hexagonal platelets with 5 atom diameter. In this microstructure, the resulting coordination of Co is complex; some platelets will overlap in the lateral and/or vertical direction, and therefore the number of nearest neighbors will strongly vary. We

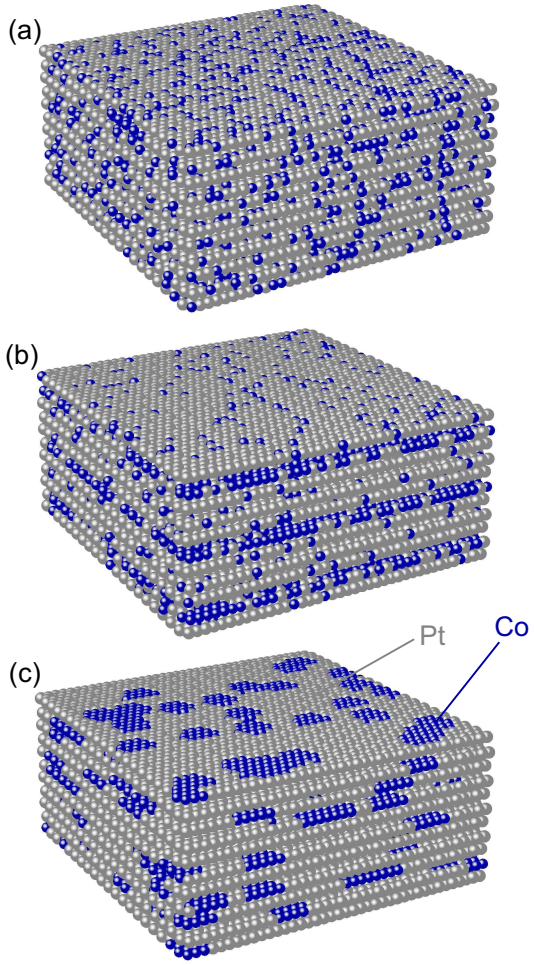

FIG. 5. Simulated structure of (a) the random fcc alloy, (b) the sub-monolayer multilayer with roughness and (c) the o-SRO film with randomly located platelets containing each 16 Co atoms. All compositions are 1:3 Co:Pt.

simulated structures with platelet size $n = 3$, 7, 11, 15, 19, 27, and 33 Co atoms (corresponding to the number of atoms included in a circle around a central atom with a radius from 1 to 3 atomic sites), in order to find the structure that best reproduces the $M(T)$ and T_C of the experiments.

The energy of the system was calculated using the Heisenberg Hamiltonian

$$H = \sum_{i \neq j} J_{ij} \vec{S}_i \cdot \vec{S}_j - \sum_i K_i (S_i^z)^2 \,, \qquad (1)$$

where $\vec{S}_i$ is a classical spin vector at site i, J_{ij} is the exchange interaction energy between first nearest neighbors, and K_i is the anisotropy constant at each site, where we assume that the strength of the anisotropy is the same at each site, i.e., $K_i \to K = \langle K_i \rangle$. The choice of the model allows us to simulate all three types of films by adjusting the anisotropy energy, *i.e.*, $K > 0$ to give out-of-plane anisotropy for the multilayer and the o-SRO

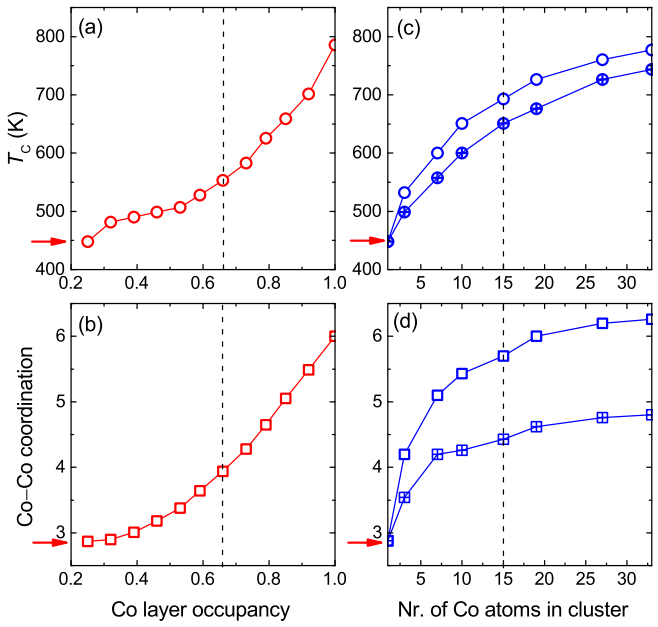

FIG. 6. Analysis of the simulated (left) multilayer and (right) o-SRO samples. Top panels show T_C and bottom panels average Co–Co coordination as a function of Co-layer occupancy (i.e. inverse roughness) in the multilayer (a and b) and platelet size in o-SRO films (c and d). In (c) and (d), open symbols show perfect platelets, and closed symbols show platelets with added roughness in the form of individual Co atoms. Red arrows indicate T_C and average coordination in the fcc alloy. The vertical dashed lines show the properties that are close to experimental values.

film and $K < 0$ to produce in-plane anisotropy (induced by shape anisotropy) for the fcc alloy film. Note that the easy magnetization axis is uniform throughout each film. It would be expected that the strength of anisotropy, i.e., the local value of K, could have local variations in Co–Pt films depending on the environment, but here we approximate that it is uniform, corresponding to the average value of K in each film, since a system with locally varying anisotropy is equivalent to a system with a uniform average anisotropy because magnetic correlation lengths are longer than inter-atomic distances. We have tested the validity of this approximation by comparing $M(T)$ curves of films with and without locally varying K, and found minimal differences, to be discussed in section V.

.

Co atoms are taken to have a spin magnetic moment of $1.75\mu_B$ (as noted above, Co also has orbital contributions to the magnetic moment at surfaces and step edges of order 0.1 to $0.2\mu_B$; as this is a comparatively small effect on either $M(T)$ or T_C, these were not included in the simulations). Taking into account that Pt becomes magnetically polarized in the vicinity of Co[60,62,63], Pt atoms which are first nearest-neighbors to a Co atom were assigned a magnetic moment of $0.3\mu_B$, second nearest-neighbors $0.2\mu_B$ and third nearest-neighbors $0.1\mu_B$, resulting in a mostly polarized Pt matrix in all cases. The choice for the Pt moments was made based on experimental observations of total moment and that the induced Pt polarization decreases with increasing distance from Co[46,64–66]. Even though these moments are comparatively small (comparable to Co orbital contributions, which we neglected), the fact that they vary from 0.1 to $0.3\mu_B$ makes them essential to include. Without this Pt polarization, the Co platelets would be superparamagnetic, and T_C would be far lower than experimentally measured.

We note that a ferromagnetic Co-Pt matrix is indicated by the experimental magnetization data (*i.e.* remanence), for the fcc alloy and the o-SRO film, which rules out any superparamagnetic behavior. In the random fcc Pt_3Co alloy, the Co concentration of 0.25 is very close to the percolation threshold in 3 dimensions (0.2488)[67], which means that without Pt polarization the phase transition would be at very low temperatures. For the o-SRO film, given that individual Co platelets are only ≈10 Å wide, consisting of 10-20 atoms, one might expect a superparamagnetic behavior (considering a Néel-Brown activation mechanism, the lifetime of the magnetic moment for a single Co platelet with these dimensions is only about 10 ns at 300 K, and 5 ns at 750 K). Stability is provided by interactions between the Co platelets, due to Pt polarization and likely single Co atoms dispersed in the Pt matrix. Time was not included in the Monte Carlo simulations shown here, hence dynamic effects will not be discussed further. The inter-platelet interactions, however, are inherent in our simulations due to the inclusion of a Pt polarization.

The values of the exchange energies were derived from experimental data, using the T_C of alloys with different composition, including Pt polarization. The T_C is linear to the total exchange energy in the system[68,69], which in a multi-sublattice system consists of the sum of interactions[70,71], hence we use the empirical relation $T_C \propto (x_{Co}^2 S_{Co}^2 J_{Co-Co} + 4x_{Pt}x_{Co}S_{Pt}S_{Co}J_{Co-Pt} + x_{Pt}^2 S_{Pt}^2 J_{Pt-Pt})$, where x_{Co} is the fraction of Co in the system, i.e., for the 1:3 alloy $x_{Co} = 1/4$ and for the 2:3 alloy it is $x_{Co} = 2/5$), and x_{Pt} is the fraction of Pt coordination. In the simulations we scaled all energies to that of Co−Co (therefore, $J_{Co-Co} = 1$, $J_{Co-Pt} = 0.78$, and $J_{Pt-Pt} = 0.69$) for simplicity. Our normalized (to J) values for the interactions are consistent with those in Ref. 72. The anisotropy constant was set to $K_{ml} = 0.1$ for the multilayer and $K_{sro} = 0.05$ for the o-SRO system, to match the experimental result $K_{ml} = 2K_{sro}$ (see values for K_{eff} Tab. II). For the random alloy, which has no perpendicular anisotropy, small in-plane anisotropy ($K_{fcc} = -0.01$) was used to mimic the shape anisotropy. We note here that while the use of classical spin simulations is better suited for systems with localized electrons, instead of itinerant systems like the alloys considered here, it is possible to describe itinerant magnets with these simulations by modifying the exchange interactions. Considering that we derive the exchange constants directly from the known Curie temperatures, this

modification is intrinsically included in our simulations.

Thermalization of the spin structure was performed using the single-spin-flip Metropolis algorithm[73,74], *i.e.*, by updating a single spin each time with a probability of $\exp(-\Delta H/T)$, where ΔH is the change in energy caused by the spin flip and T is the temperature. 10^4 Monte Carlo steps per site (MCS) were run to reach equilibrium, and then an additional 10^4 MCS were taken to obtain the average spontaneous magnetization, which is the vector sum of all magnetic moments in the system, at each temperature. The simulation was started at $T = 0$ with full polarization, and the equilibrium state and M of the system was calculated at each temperature step upon heating from 0 to 850 K with a step of 10 K.

The lateral size of the systems was $L \times L = 80 \times 80$, and the thickness was $D = 11$ atomic planes. Periodic boundary conditions were used in the lateral dimensions to eliminate finite size effects, whereas free boundaries were assumed for the surfaces. Occasional checks were performed with smaller and larger systems ($L = 60$ and $L = 128$) to verify the validity of the results.

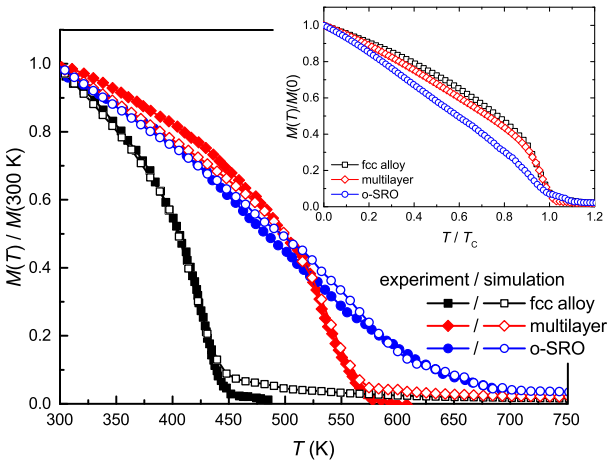

FIG. 7. Comparison between experimental (full symbols) and simulated (open symbols) magnetization as a function of temperature (M normalized to the room-temperature value) for the random fcc alloy (black squares), the multilayer (red diamonds), and o-SRO $CoPt_3$ film with 20% roughness (blue circles). The inset shows the normalized M as a function of normalized temperature, in order to illustrate the difference of $M(T)$.

V. MONTE CARLO SIMULATIONS: RESULTS AND DISCUSSION

Figure 6 shows the Curie temperature T_C and the average Co-Co coordination in (left panels) the multilayer as a function of Co occupancy in the Co plane and (right panels) in the o-SRO film as a function of platelet size. Co occupancy in the multilayer is defined as the fraction of Co atoms in the Co layer, hence increasing roughness causes decreasing occupancy; e.g. an occupancy of 1 corresponds to a perfect fully occupied Co layer, with no roughness. Roughness decreases the Co occupancy below 1; for the 1:3 Co:Pt ratio here considered, the lower limit of the occupancy is 0.25 in which case all layers then have the same Co occupancy, *i.e.*, like in the random fcc alloy. For the platelets, the smallest platelet is $n = 1$, which corresponds to the random fcc alloy.

In the multilayer structure, Fig. 6 shows that the average coordination and (consequently) T_C increases quadratically with increasing occupancy/decreasing roughness. For zero roughness, occupancy = 1, T_C = 800 K, less than the full T_C of Co due to the reduced Co-Co coordination of the thin Co layer (but greater than a 2D layer of Co due to Pt polarization in the neighboring layers). In order to have a T_C close to 570 K, as measured in the experiments, the occupancy must be between 0.6 and 0.7, near the 0.72 of the perfect sub-ML multilayer.

In the o-SRO film, T_C starts at 450 K in the fcc ($n = 1$) limit (single Co atoms), then increases steadily with increasing platelet size; for platelets with 15 Co atoms or more it approaches the 800 K limit of a full Co-layer. From Fig. 6(c) we see that in order to reproduce the T_C observed in the experiments on the o-SRO films, we need a structure with Co platelets containing 15 atoms, which corresponds to platelets with roughly 1 nm by 1 nm in size, in good agreement with EXAFS findings. We have also considered o-SRO films with roughness in the form of individual Co atoms dispersed in the matrix, and we compare in Fig. 6 the T_C, which is lower than that of films with perfect platelets. For this example we constructed the o-SRO structure using the same algorithm described above, and then randomly relocated some % of the Co atoms to new locations, thus diluting the platelets. Roughness thus plays an important role in both multilayers and o-SRO films.

We now compare the experimental and simulated $M(T)$ of the fcc alloy, a sub-ML multilayer (with additional roughness: 0.65 occupancy, chosen to match T_C of the experimental 1:3 sub-ML multilayer film), and an o-SRO film with platelets containing 15 Co atoms and 20% roughness (chosen to match T_C and linear-like shape of the experimental data). The agreement between simulation and experiment confirms the validity of the simulated structures shown in Fig. 5, especially considering the stretched $M(T)$ of the o-SRO film and the Langevin-like $M(T)$ of the multilayer and fcc alloy. The normalized $M(T)$ of the three structures is shown in the inset to Fig. 7. The $M(T)$ of the fcc and multilayer are almost identical, whereas that of the o-SRO film is completely different, and lies below the $M(T)$ of the fcc or the multilayer sample, similar to the experimental data shown in the inset to Fig. 5.

While the simulations qualitatively reproduce the shape of $M(T)$ and reasonable values of T_C for all three samples, the total magnetic moment in each sample and particularly the enhancement in M for the o-SRO films are not reproduced by the Monte Carlo simulations. This

is because the Co moment was held constant in this simulation, while it is known that Co at Pt surfaces has a significant orbital moment, and Co at step edges a still further enhanced value, as discussed in the experimental section.

The key component, which causes different $M(T)$ behavior in the three systems, is the difference in the distribution of Co-Co coordination in each system. These distributions are calculated for each structure and shown in Fig. 8; from the distribution, we calculate the average Co-Co coordination number z and the width of the distribution. In all cases, in the fcc lattice the maximum number of possible nearest neighbors is 12. For the simulated random fcc alloy (Fig. 8a), the distribution is a Gaussian, as expected given the random site occupation, with $z = 2.88$ (the theoretical value is 3, for a composition of 1:3) and a distribution width of 3.1. For the sub-ML multilayer (Fig. 8b), $z = 3.95$; the distribution is also Gaussian with a width of 3.9. Note that for a fully occupied (111) plane with zero roughness, $z = 6$; this number is here reduced and a distribution created because the occupancy was reduced to simulate the sub-ML character of the experimental multilayer, and roughness introduced such that we get a T_C that agrees with the experiment. For the o-SRO alloy with 15-atom clusters (Fig. 8c), $z = 5.63$; the distribution does not follow a Gaussian form, but is broader than the other two, with significant values at 6, and some even at 12 (well above the maximum value of 6 for an isolated ML platelet of Co atoms), indicating platelets lying on top of each other. This large average coordination and wider distribution yields the higher T_C and non-Langevin $M(T)$ of the o-SRO compared to the sub-ML multilayer.

We further illustrate this effect by looking at a o-SRO film with the smallest platelets ($n = 3$), and comparing its $M(T)$ to that of the random fcc alloy (Fig. 9a). The clustering of the Co atoms, and the fact that some 3-atomic clusters are in contact, thus creating larger structures, generates a more inhomogeneous distribution of Co–Co bonds, and causes $M(T)$ to depart from the typical Langevin-like shape. Additionally, we compare an o-SRO film with 15-atom platelets, i.e., the structure that has T_C similar to the experimental value, and an o-SRO film with the same platelet size but with additional roughness in the form of individual Co atoms dispersed in the lattice, specifically 20% of these, chosen to best match the experimental $M(T)$ (see Fig. 9b). As seen in fig. 9(b) the additional roughness further changes the shape of $M(T)$, which becomes increasingly linear, similar to the experimentally observed curve. Hence from our simulations we infer that the combination of non-uniform Co–Co coordination and roughness is responsible for the nearly linear shape of $M(T)$ found in the experiment.

Turning to the effects of Co-Co coordination on the anisotropy of each film, we compare the in-plane coordination (α) and the out-of-plane coordination (β), where the difference $\alpha-\beta$ is a measure of the PMA in the system (for details see Ref. 51). Similar to Ref. 51, we define α

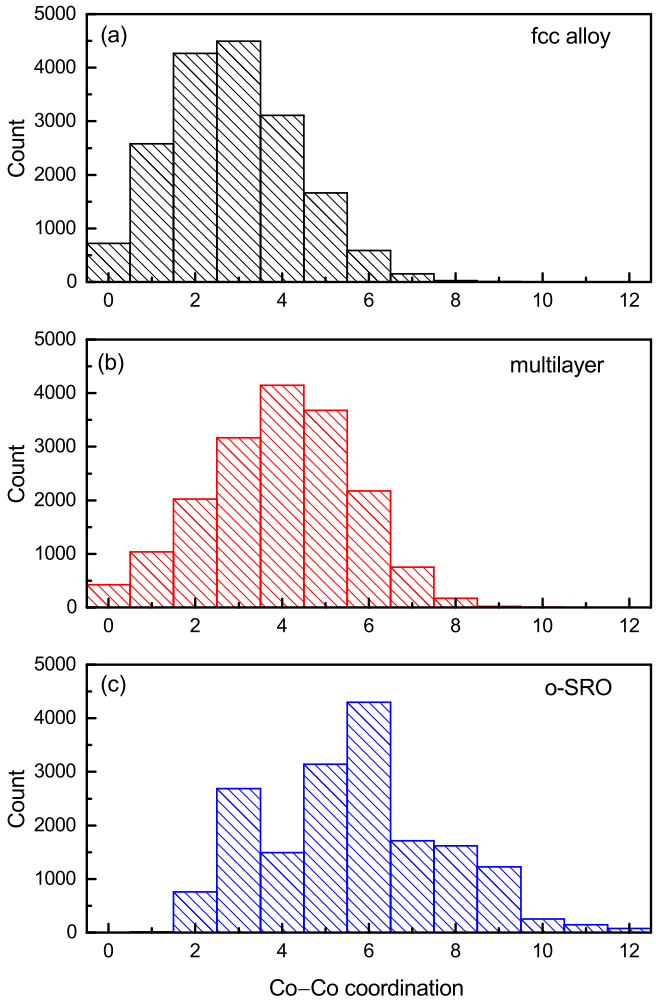

FIG. 8. Distribution of number of Co-Co nearest neighbors (in-plane and out-of-plane here combined) in (a) the random fcc alloy, (b) the rough sub-ML multilayer, and (c) the o-SRO film with platelets containing 15 Co atoms.

as the fraction of the six in-plane nearest-neighbor (NN) sites occupied by Co, and β as the fraction of the six out-of plane NN sites occupied by Co, so that $\alpha - \beta$ is a measure of the structural anisotropy. For the simulated random fcc alloy, the structure has $\alpha = 0.24$ and $\beta = 0.23$ leading to $\alpha - \beta = 0.01$, which is close to the ideal value of 0 (no in- or out-of-plane preference in the random structure), confirming that our algorithm for the structure generation is correct. Turning to the multilayer samples, we note that $\alpha - \beta$ would reach unity in a perfectly layered film, where the Co occupation of the Co plane is 1, so $\alpha = 1$ and $\beta = 0$, so $\alpha - \beta = 1$. The multilayer here simulated (sub-ML, with roughening) has $\alpha = 0.504$, $\beta = 0.153$, and $\alpha - \beta = 0.351$, non-zero, but strongly reduced from 1.0. Turning to the o-SRO film with $n = 15$ and no roughness, we find $\alpha = 0.724$ and $\beta = 0.214$, leading to $\alpha-\beta = 0.509$, larger than the value of the multilayer, a result inconsistent with experimental magnetic anisotropy results (the multilayer has larger

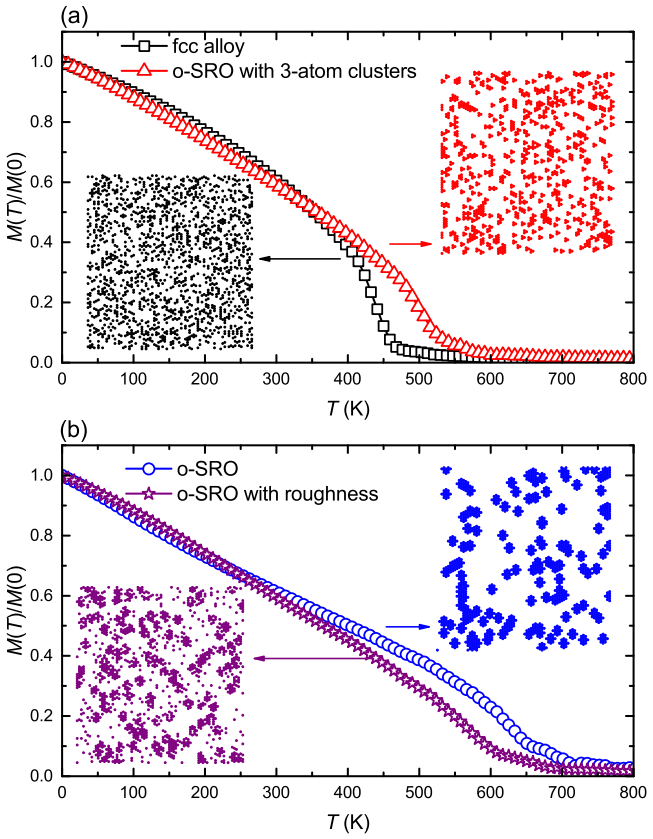

FIG. 9. (a) Comparison between the simulated magnetization as a function of temperature for the fcc alloy (black squares) and an o-SRO film with 3-atomic clusters (red triangles), showing that even 3-atom clusters are sufficient to distort $M(T)$ compared to the random alloy. Inserts show top-view of an atomic plane in each structure, with black circles representing Co atoms in the fcc alloy (bottom-left insert) and red triangles representing the 3-Co-atom clusters in the o-SRO film (top-right insert). (b) Comparison between the $M(T)$ of an o-SRO film with 15-atom clusters (blue circles) and the same film with 20% induced roughness (purple stars), showing that roughness plays a very important role in the shape of $M(T)$, i.e., with increasing roughness the magnetization becomes increasingly linear with T, despite little effect on T_C. The top-right and bottom-left inserts of (b) show a top-view of the Co structure in the o-SRO film without and with roughness, respectively.

PMA than the o-SRO film). This is due to the deliberate roughness introduced to the multilayer; the discrepancy can be reconciled by introducing 20% roughness [as previously discussed, this value gives the best match to both T_C and $M(T)$] also in the o-SRO film (see Fig. 9b), which leads to $\alpha - \beta = 0.279$, very close to the theoretical value of 0.26 found from growth simulations[51], and more compatible with the PMA values.

We note that the enhanced moments of edge and surface Co atoms introduced by platelets and roughness would increase the strength of the interactions and hence the T_C, so it is likely that a suitable mixture of roughness and platelet size, combined with the enhanced Co moments at surfaces and edges, could be found to match all parameters [T_C, K_u, M_S and $M(T)$] but that optimization was not here undertaken. Moreover, the *local* variation of the anisotropy from site to site could also play a role in the shape of $M(T)$, but the exact determination of the on-site anisotropy would have to be calculated with ab-initio methods, which are out of the scope of this study. We did, however, test a spatially varying anisotropy, the *local* strength of which is proportional to the magnitude of the structural anisotropy $(\alpha - \beta)$ at each Co site, and we found no significant deviation from the results shown here obtained by considering a uniform anisotropy strength acting on all Co atoms.

VI. CONCLUSION

We have shown that ultrathin (Co/Pt) multilayers and o-SRO $CoPt_3$ films exhibit very different temperature-dependence of magnetization, arising from different geometries of local atomic configuration. The stretched experimental $M(T)$ curve, enhanced M_s, and enhanced T_C of the o-SRO films can only be explained by thin platelets (1-2 layers thick) with a width of 10 Å to 20 Å and Pt polarization-induced exchange coupling between platelets separated by thicknesses from 1-3 Pt monolayers. Monte Carlo simulations show that the shape of the experimental $M(T)$ of the $CoPt_3$ alloy containing small in-plane Co platelets is due to a broad distribution of Co-Co coordination, and that to obtain the experimentally observed Curie temperatures requires roughening of the multilayer structure and a platelet size of approximately 15 atoms $\approx$ 10 Å diameter in the o-SRO film, consistent with both growth simulations and EXAFS measurements in the literature. The enhanced magnetization of the o-SRO films with PMA is a consequence of Co atoms at edges of platelets, consistent with the 15 atom platelet size, evidence therefore of the imperfect nature of the platelets, which is nonetheless enough to give rise to PMA that is nearly that of a perfect multilayer.

ACKNOWLEDGMENTS

The characterization, simulation and analysis part of this work was supported by the Director, Office of Science, Office of Basic Energy Sciences, Materials Sciences and Engineering Division, of the U.S. Department of Energy under Contract No. DE-AC02-05-CH11231 within the Non-Equilibrium Magnetic Materials Program. Sample preparation and magnetic characterization was supported by the Director, Office of Science, Office of Basic Energy Sciences, Materials Sciences and Engineering Division, of the U.S. Department of Energy under Contract No. DE-FG02-04ER46100. This work also benefited from computer-time Grants #2008001 and #2012007 of

the Centre de Resources Informatiques de Haute Normandie (CRIHAN).

* Current address: NIST Center for Neutron Research, Gaithersburg, MD 20899, USA
† fhellman@berkeley.edu

[1] P. F. Carcia, J. Vac. Sci. Technol. A **5**, 1975 (1987).
[2] P. F. Carcia, J. Appl. Phys. **63**, 5066 (1988).
[3] N. Nakajima, T. Koide, T. Shidara, M. Miyauchi, H. Fukutani, A. Fujimori, K. Iio, T. Katayama, M. NÃ$\frac{1}{2}$vlt and Y. Suzuki, Phys. Rev. Lett. **81**, 5229 (1998).
[4] S. J. Yuan, L. Sun, H. Sang, J. Du and S. M. Zhou, Phys. Rev. B **68**, 134443 (2003).
[5] D. Weller, Y. Wu, J. Stöhr, M. G. Samant, B. D. Hermsmeier and C. Chappert, Phys. Rev. B **49**, 12888 (1994).
[6] J. M. MacLaren and R. H. Victora, Appl. Phys. Lett. **66**, 3377 (1995).
[7] N. Nakamura, H. Ogi and M. Hirao, Appl. Phys. Lett. **86**, 111918 (2005).
[8] M. Ota, M. Itou, Y. Sakurai, A. Koizumi and H. Sakurai, Appl. Phys. Lett. **96**, 152505 (2010).
[9] S. Bandiera, R. C. Sousa, B. Rodmacq and B. Dieny, Appl. Phys. Lett. **100**, 142410 (2012).
[10] O. Hellwig, T. L. Kirk, J. B. Kortright, A. Berger and E. E. Fullerton, Nature Materials **2**, 112 (2003).
[11] R. Frömter, H. Stillrich, C. Menk and H. P. Oepen, Phys. Rev. Lett. **100**, 207202 (2008).
[12] Y. L. Iunin, Y. P. Kabanov, V. I. Nikitenko, X. M. Cheng, D. Clarke, O. A. Tretiakov, O. Tchernyshyov, A. J. Shapiro, R. D. Shull and C. L. Chien, Phys. Rev. Lett. **98**, 117204 (2007).
[13] P. J. Metaxas, P. J. Zermatten, J. P. Jamet, G. G. J. Ferré, A. S. B. Rodmacq and R. L. Stamps, Appl. Phys. Lett. **94**, 132504 (2009).
[14] J. E. Davies, O. Hellwig, E. E. Fullerton, M. Winklhofer, R. D. Shull and K. Liu, Appl. Phys. Lett. **95**, 022505 (2009).
[15] Y. L. Iunin, Y. P. Kabanov, V. I. Nikitenko, X. M. Cheng, C. L. Chien, A. J. Shapiro, R. D. Shull, J. Magn. Magn. Mater. **320**, 2044 (2008).
[16] A. Berger, S. Mangin, J. McCord, O. Hellwig and E. E. Fullerton, Phys. Rev. B **82**, 104423 (2010).
[17] W. B. Zeper and F. J. A. M. Greidanus, J. Appl. Phys. **65**, 4971 (1989).
[18] S. Uba, L. Uba, A. N. Yaresko, A. Y. Perlov, V. N. Antonov and R. Gontarz, Phys. Rev. B **53**, 6526 (1996).
[19] S. Fiedler, H. Stillrich and H. P. Oepen, J. Appl. Phys. **102**, 83906 (2007).
[20] Š. Višňovský, E. J. Lišková, M. Nývlt and R. Krishnan, Appl. Phys. Lett. **100**, 232409 (2012).
[21] J. W. Knepper and F. Y. Yang, Phys. Rev. B **71**, 224403 (2005).
[22] Z. Y. Liu, F. Zhang, H. L. Chen, B. Xu, D. L. Yu, J. L. He and Y. J. Tian, Phys. Rev. B **79**, 024427 (2009).
[23] A. Aziz, S. J. Bending, H. G. Roberts, S. Crampin, P. J. Heard and C. H. Marrows, Phys. Rev. Lett. **97**, 206602 (2006).
[24] C. L. Canedy, X. W. Li and G. Xiao, Phys. Rev. B **62**, 508 (2000).
[25] J. Y. Zhang, Z. L. Wu, S. G. Wang, C. J. Zhao, G. Yang, S. L. Zhang, Y. Liu, S. Liu, J. Teng and G. H. Yu, Appl. Phys. Lett. **102**, 102404 (2013).
[26] E. Shipton, K. Chan, T. Hauet, O. Hellwig and E. E. Fullerton, Appl. Phys. Lett. **95**, 132509 (2009).
[27] J. Y. Chen, J. F. Feng, Z. Diao, G. Feng, J. M. D. Coey and X. F. Han, IEEE Trans. Mag. **46**, 1401 (2010).
[28] L. Grenet, M. Jamet, P. Noé, V. Calvo, J. M. Hartmann, L. E. Nistor, B. Rodmacq, S. Auffret, P. Warin and Y. Samson, Appl. Phys. Lett. **94**, 032502 (2009).
[29] A. Rajanikanth, S. Kasai, N. Ohshima and K. Hono, Appl. Phys. Lett. **97**, 22505 (2010).
[30] S. Emori and G. S. D. Beach, J. Appl. Phys. **110**, 033919 (2011).
[31] D. Houssameddine, U. Ebels, B. Delaët, B. Rodmacq, I. Firastrau, F. Ponthenier, M. Brunet, C. Thirion, J. P. Michel, L. Prejbeanu-Buda, M.-C. Cyrille, O. Redon and B. Dieny, Nature Materials **6**, 447 (2007).
[32] L. San Emeterio Alvarez, K.-Y. Wang, S. Lepadatu, S. Landi, S. J. Bending, and C. H. Marrows, Phys. Rev. Lett. **104**, 137205 (2010).
[33] S. Mangin, D. Ravelosona, J. A. Katine, M. J. Carey, B. D. Terris and E. E. Fullerton, Nature Materials **5**, 210 (2006).
[34] L. Piraux, V. A. Antohe, F. Abreu Araujo, S. K. Srivastava, M. Hehn, D. Lacour, S. Mangin and T. Hauet, Appl. Phys. Lett. **101**, 013110 (2012).
[35] S. Ishikawa, H. Sato, M. Yamanouchi, S. Ikeda, S. Fukami, F. Matsukura and H. Ohno, J. Appl. Phys. **113**, 17C721 (2013).
[36] K. Wang, M.-C. Wu, S. Lepadatu, J. S. Claydon, C. H. Marrows, and S. J. Bending, J. Appl. Phys. **110**, 083913 (2011).
[37] J. Vogel, M. Bonfim, N. Rougemaille, O. Boulle, I. M. Miron, S. Auffret, B. Rodmacq, G. Gaudin, J. C. Cezar, F. Sirotti, and S. Pizzini, Phys. Rev. Lett. **108**, 247202 (2012).
[38] A. Hrabec, N. A. Porter, A. Wells, M. J. Benitez, G. Burnell, S. McVitie, D. McGrouther, T. A. Moore, and C. H. Marrows, Phys. Rev. B. **90**, 020402(R) (2014).
[39] S.-G. Je, D.-H. Kim, S.-C. Yoo, B.-C. Min, K.-J. Lee, and S.-B. Choe, Phys. Rev. B **88**, 214401 (2013).
[40] A. A. Fraerman, O. L. Ermolaeva, E. V. Skorohodov, N. S.Gusev, V. L. Mironov, S. N. Vdovichev, E. S. Demidov, J. Magn. Magn. Mater. **393**, 452 (2015).
[41] C. Moreau-Luchaire, C. Moutafis, N. Reyren, J. Sampaio, C. A. F. Vaz, N. Van Horne, K. Bouzehouane, K. Garcia, C. Deranlot, P. Warnicke, P. Wohlhüter, J.-M. George, M. Weigand, J. Raabe, V. Cros, and A. Fert, Nature Nano. (2016) doi:10.1038/nnano.2015.313
[42] S. Woo, K. Litzius, B. Krüger, M.-Y. Im, L. Caretta, K. Ritchter, M. Mann, A. Krone, R. Reeve, M. Weigand, P. Agrawal, P. Fischer, M. Kläui, G. S. D. Beach, Nature Materials (2016) doi:10.1038/nmat4593
[43] N. W. E. McGee, M. T. Johnson, J. J. de Vries, and J. aan de Stegge, J. Appl. Phys. **73**, 3418 (1993).
[44] C. S. Shern, J. S. Tsay, H. Y. Her, Y. E. Wu, and R. H. Chen, Surf. Sci. **429**, L497 (1999).
[45] P. W. Rooney, A. L. Shapiro, M. Q. Tran, and F. Hellman, Phys. Rev. Lett. **75**, 1843 (1995).

[46] A. L. Shapiro, P. W. Rooney, M. Q. Tran, F. Hellman, K. M. Ring, K. L. Kavanagh, B. Rellinghaus, and D. Weller, Phys. Rev. B **60**, 12826 (1999).

[47] B. B. Maranville and F. Hellman, Appl. Phys. Lett. **79**, 2782 (2001).

[48] D. Vasumathi, B. B. Maranville, and F. Hellman, Appl. Phys. Lett. **81**, 4011 (2002).

[49] T. A. Tyson, S. D. Conradson, R. F. C. Farrow, and B. A. Jones, Phys. Rev. B **54**, R3702(R) (1996).

[50] J. O. Cross, M. Newville, B. B. Maranville, C. Bordel, F. Hellman, and V. G. Harris, J. Phys.: Condens. Matter **22**, 146002 (2010).

[51] B. B. Maranville, M. Schuermann and F. Hellman, Phys. Rev. B **73**, 104435 (2006).

[52] H. Berg and J. B. Cohen, Met. Trans. **3**, 1797 (1972).

[53] P. Grütter and U. T. Dürig, Phys. Rev. B **49**, 2021 (1994).

[54] J. Kim, J. W. Lee, J. R. Jeong, and S. C. Shin, Phys. Rev. B **65**, 104428 (2002).

[55] C. Klein, R. Koller, E. Lundgren, F. Maca, J. Redinger, M. Schmid, and P. Varga, Phys. Rev. B **70**, 153403 (2004).

[56] T. Das, P. D. Kulkarni, S. C. Purandare, H. C. Barshilia, S. Bhattacharyya, P. Chowdhury, Sci. Rep. **4**, 5328 (2014).

[57] J. Chatterjee, T. Tahmasebi, S. Mertens, G. S. Kar, T. Min, J. De Boeck, IEEE Trans. Magn. **50**, 4401704 (2014).

[58] S. Rüegg, G. Schütz, P. Fischer, R. Wienke, W. B. Zeper, H. Ebert, J. Appl. Phys. **69**, 5655 (1991).

[59] J. Geissler, E. Goering, M. Justen, F. Weigand, G. Schütz, J. Langer, D. Schmitz, H. Maletta, and R. Mattheis, Phys. Rev. B **65**, 020405(R) (2001).

[60] J. Crangle and W. R. Scott, J. Appl. Phys. **36**, 921 (1965).

[61] A. Ney, P. Poulopoulos, and K. Baberschke, Europhys. Lett. **54**, 820 (2001).

[62] W. Grange, M. Maret, J.-P. Kappler, J. Vogel, A. Fontaine, F. Petroff, G. Krill, A. Rogalev, J. Goulon, M. Finazzi, and N. B. Brookes, Phys. Rev. B **58**, 6298 (1998).

[63] R. E. Parra and R. A. López, J. Appl. Phys. **61**, 3989 (1987).

[64] W. Grange, I. Galanakis, M. Alouani, M. Maret, J.-P. Kappler, A. Rogalev, Phys. Rev. B **62**, 1157 (2000).

[65] H. Ebert, S. Ruegg, G. Schütz, R. Wienke, W. B. Zeper, J. Magn. Magn. Mater. **93**, 601–604 (1991).

[66] M. Suzuki, H. Muraoka, Y. Inaba, H. Miyagawa, N. Kawamura, T. Shimatsu, H. Maruyama, N. Ishimatru, Y. Isohama, Y. Sonobe, Phys. Rev. B **72**, 054430 (2005).

[67] C. D. Lorentz and R. M. Ziff, Phys Rev. E **57**, 230 (1998)

[68] P. Peczak, A. M. Ferrenberg, D. P. Landau, Phys. Rev. B **43**, 6087 (1991).

[69] C. Holm and W. Janke, Phys. Rev. B **48**, 936 (1993).

[70] P. W. Anderson (1963), Theory of Magnetic Exchange Interactions: Exchange in Insulators and Semiconductors, in Solid State Physics, edited by F. Seitz and Turnbull (Academic Press, New York), Vol. 14, pp. 99-214.

[71] E. Şaşioğlu, L. M. Sandratskii, and P. Bruno, Phys. Rev. B **70**, 024427 (2004).

[72] J. M. Sanchez, J. L. Morán-López, C. Leroux, M. C. Cadeville, J. Phys.: Condens. Matter **1**, 491–496 (1989).

[73] N. Metropolis, A. Rosenbluth, M. Rosenbluth, A. Teller and E. Teller, J. Chem. Phys. **21**, 1087 (1953).

[74] K. Binder and D. Heermann, Monte Carlo Simulation in Statistical Physics (Second ed., Springer, 1990).